Development of a Lifting-Line-Based Method for Preliminary Propeller Design

Conference Paper · June 2018

DOI: 10.1115/OMAE2018-77995

5 authors, including:

Jose Rodolfo Chreim
Instituto de Pesquisas Tecnológicas
17 PUBLICATIONS **19** CITATIONS
SEE PROFILE

Gustavo R S Assi
University of São Paulo
80 PUBLICATIONS **772** CITATIONS
SEE PROFILE

João Lucas Dozzi Dantas
Instituto de Pesquisas Tecnológicas
92 PUBLICATIONS **236** CITATIONS
SEE PROFILE

Eduardo Tadashi Katsuno
University of São Paulo
35 PUBLICATIONS **65** CITATIONS
SEE PROFILE

Proceedings of the ASME 2018 37th International Conference onf Ocean, Offshore and Arctic Engineering
OMAE 2018
June 17-22, 2018, Madrid, Spain

OMAE2018-77995

DEVELOPMENT OF A LIFTING-LINE-BASED METHOD FOR PRELIMINARY PROPELLER DESIGN

Jose Rodolfo Chreim *
Marcos de Mattos Pimenta
Department of Mechanical Engineering
Polytechnique School
University of Sao Paulo
Sao Paulo, Sao Paulo 05508-900
Brazil
Email: jrchreim@usp.br

Joao Lucas Dozzi Dantas

Naval and Ocean Engineering Laboratory
IPT - Institute for Technological Research
Sao Paulo, Sao Paulo, 05508-901
Brazil
Email: jdantas@ipt.br

Gustavo R. S. Assi

Department of Naval and Oceanic Engineering
Polytechnique School
University of Sao Paulo
Sao Paulo, Sao Paulo, 05508-901
Brazil
Email: g.assi@usp.br

Eduardo Tadashi Katsuno

Department of Mechanical Engineering
Polytechnique School
University of Sao Paulo
Sao Paulo, Sao Paulo 05508-900
Brazil
Email: eduardo.katsuno@usp.br

ABSTRACT

A novel formulation for marine propellers based on adaptations from wing lifting-line theory is presented; the method is capable of simulating propellers with skewed and raked blades. It also incorporates the influence of viscosity on thrust and torque from hydrofoil data through a nonlinear scheme that changes the location of the control points iteratively. Several convergence studies are conducted to verify the different aspects of the numerical implementation and the results indicate satisfactory convergence rates for Kaplan, KCA, and B-Troost propellers. It is expected that the method accurately describes thrust, torque, and efficiency under the moderately loaded propeller assumption.

KEYWORDS: Propeller Lifting-Line, Propeller Analysis, Propeller Design, Vortex Step Method

NOMENCLATURE

c Blade section chord.
C_c Hydrofoil axial force coefficient.
C_n Hydrofoil normal force coefficient.
C_{n_α} Hydrofoil normal force slope $\frac{\partial c_n}{\partial \alpha}$.
D Propeller diameter.
D_P Pressure Drag due to the hub.
$\vec{e}_{aP}$ Propeller axial unit vector.
$\vec{e}_{nP}$ Propeller normal unit vector.
K_T Propeller thrust coefficient.
K_Q Propeller torque coefficient.
N Number of dicretizations for each blade.
N_B Number of blades.
$\vec{R}$ Vector radius of a given control point or vortex edge.
R_h Hub radius.

*Address all correspondence to this author.

R_0 Core radius of the Rankine Vortex.
$\vec{R}_{Im}$ Vector radius of an image vortex.
Re Reynolds number.
$\vec{r}$ Vector from trailing vortex edge to a point in space.
$\vec{u}_n$ Normal-to-the-blade-planform unit vector.
$\vec{v}_a$ axial component of the induced velocity.
$\vec{V}_{HS}$ Velocity induced by a horseshoe.
$\vec{V}_{Ind}$ Overall induced velocity over a control point.
$\vec{V}_\infty$ Free-stream velocity
$\vec{V}_P$ Overall velocity on a control point.
$\vec{V}_{VS}$ Velocity induced by a vortex segment.
$\vec{V}_t$ Tangential velocity of a control point.
$\vec{v}_t$ tangential component of the induced velocity.
$\vec{V}_{TV}$ Velocity due to the trailing vortices.
W_∞ Normal component of the overall velocity $\vec{V}_P$.
x Chordwise location of the control point
α_{eff} Effective angle of attack.
α_{L0} Zero lift angle of attack.
β Pitch angle at a given control point.
β_{Ind} Induced pitch angle at a given control point.
β_W Pitch angle at a trailing vortex.
$\vec{\delta}_l$ Spatial vector along a given bound segment.
δ_A Planform area of a given blade section.
Γ Circulation distribution.
Ω Relaxation factor.
$\vec{\omega}$ Propeller rotational speed.
ρ Free-stream density.
θ Angle between $\vec{V}_{TV}$ and $\vec{\delta}_l$.
b_* Superscript denoting the $*^{th}$ blade.
i Subscript denoting i^{th} control point.
j Subscript denoting j^{th} horseshoe vortex.
k_* Subscript denoting the k_*^{th} segment of the horseshoe vortex.

INTRODUCTION

In the last years, the increased knowledge in the emission estimates for greenhouse gases from ships made the International Maritime Organization (IMO) adopt an Energy Efficiency Design Index (EEDI) for the design of ships. Within this context, ship design requires the design of efficient performance propellers too, a complex process that demands the use of several auxiliary tools; while many are available, there is usually a compromise between detail and cost, which makes each of them more adequate for a specific phase: Systematic series, although fast, are limited in flexibility; lifting-line (LL) tools are generally limited to potential flows and simple geometries (that can transformed to more complex ones with lifting-surface coupling); and commercial CFD software are capable of simulating complex flows and geometries, but at a rather high computational cost.

The propeller LL (PLL) started concomitantly with the wing LL (WLL) theory of Lanchester and Prandtl; it was initially limited to infinite-bladed propellers as a means to circumvent the influence of the complex helical wake. Only in 1936, Kawada [1] managed to calculate the velocities induced by this geometry, enabling the PLL to be used with a finite number of blades. While Kawada represented the blades by lines of constant vorticity, Lerbs [2] extended such representation to varying strength bound vortex lines that, to satisfy Kelvins Circulation Theorem, shed sheets of trailing vortices onto the free-stream. His formulation is similar to the classical WLL of Lanchester and Prandtl.

As the results of the PLL were not sufficiently accurate, Morgan et al. obtained correction factors based on the results of the lifting-surface (LS) theory from Cheng and Kerwin and Leopold [3]. These correction factors improved the results obtained by the PLL methods.

The Massachussets Institute of Technology conducted much research related to the formulation of Lerbs and the work of Kerwin that later coalesced into a numerical tool: *OpenProp* [4] is a PLL software (with corrections from LS) for the design and analysis of marine propellers and horizontal-axis turbines with many capabilities. Although having design and analysis capabilities, a generalized model for rotors with rake and skew is a planned enhancement.

Similar to Openprop, *IndFact* [5], a PLL program based on Lerbs formulation and Morgans LS corrections, was developed by the Maritime Research Institute Netherlands (MARIN). According to the developers, the accuracy of IndFact is within a few percent. No open information is provided about the tool for the case of nonsymmetrical wake and geometries with rake and skew.

The formulation of Lerbs, although suitable for preliminary design, is limited to the case of potential flows over blades with no rake and skew, and even under these circumstances, the results must be improved with corrections from lifting-surface theory. Even though viscosity can be incorporated on torque [6], its effects on thrust are not accounted. On the other hand, advances in WLL were such that most of the mentioned limitations have been overcome [7–10]. Therefore, the current paper presents a novel PLL formulation that allows for the analysis of *skewed* and/or *raked* propellers; moreover, it considers the influence of viscosity on thrust and torque by way of incorporating real hydrofoil data through a nonlinear formulation. The final purpose is to have a more robust, yet still fast, propeller lifting-line formulation, capable of simulating complex geometries and the influence of viscosity, and setting aside the need for lifting-surface corrections.

FORMULATION

Divided into linear and nonlinear formulations, the present Propeller lifting-line method is inspired on the works of Epps [4],

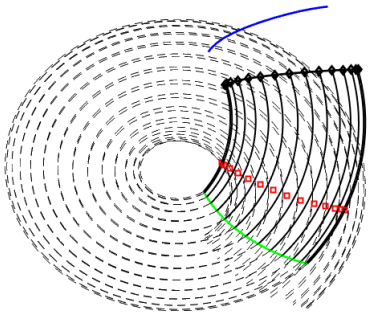

FIGURE 1. Representation of the propeller blade by a series of HSVs. The bold black lines are part of the HSVs that are over the planform, while the dashed lines represent part of the trailing vortices that are shed following a helical path.

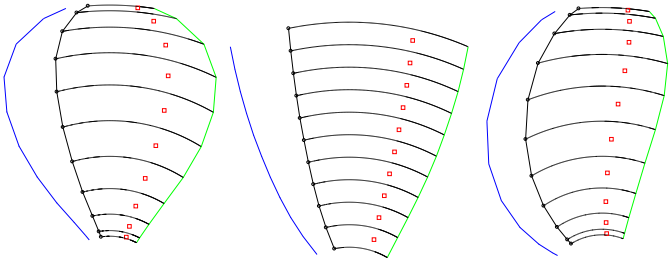

FIGURE 2. Blade discretization. From left to right: KCA (CHCP clustering), Kaplan (EHEP clustering), and B-Troost (CHCP clustering). The figure shows: the leading and trailing edges; the bound vortices and parts of the trailing vortices that remain over the planform; and the control points.

Katz & Plotkin [7], Kerwin [6], Phillips & Snyder [8], and Souza [9], and it is an adaptation of modern wing lifting-line methods. Considerations about the wake and the hub are also presented.

Linear Formulation

In the current model, a propeller blade b_j and its wake are represented by a series of N horseshoe vortices (HSV) as in Fig. 1; The HSVs bound segments lay over the blade $\frac{c}{4}$ line, and part of the wake remains over its planform (Fig. 2), while the other part is shed following a helical path.

While there is no analytical expression to the induced velocity of such HSV, the complex geometry can be approximated by a series of straight vortex segments, so as the number of straight segments increases the solution tends to the theoretical one (Fig. 3).

The velocity of the segment j, with vertices k_j and k_{j+1} and

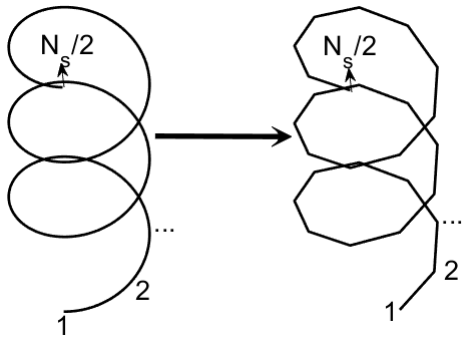

FIGURE 3. Approximation of the proposed HSV by a series of straight vortex segments.

circulation $\Gamma_j^{b_j}$, on a point i from blade b_i can be analitically calculated with the aid of Eqn. (1) [7, 8]:

$$\vec{V}_{VS_{ij,k_jk_{j+1}}^{b_ib_j}} = \frac{\Gamma_j^{b_j}}{4\pi} \frac{\left(r_{ij,k_j}^{b_ib_j} + r_{ij,k_j+1}^{b_ib_j}\right)\left(\vec{r}_{ij,k_j}^{b_ib_j} \times \vec{r}_{ij,k_j+1}^{b_ib_j}\right)}{r_{ij,k_j}^{b_ib_j} r_{ij,k_j+1}^{b_ib_j}\left(r_{ij,k_j}^{b_ib_j} r_{ij,k_j+1}^{b_ib_j} + \vec{r}_{ij,k_j}^{b_ib_j} \cdot \vec{r}_{ij,k_j+1}^{b_ib_j}\right)} \tag{1}$$

such that the velocity of the entire horseshoe over i is given by the sum of all the individual contributions, according to the principle of superposition:

$$\vec{V}_{HS_{ij}^{b_ib_j}} = \frac{1}{4\pi}\sum_{k_j=1}^{N_S} \vec{V}_{VS_{ij,k_jk_j+1}^{b_ib_j}} = \frac{\Gamma_j^{b_j}}{4\pi}\vec{v}_{ij}^{b_ib_j} \tag{2}$$

$$\vec{v}_{ij}^{b_ib_j} = \sum_{k_j=1}^{N_S} \frac{\left(r_{ij,k_j}^{b_ib_j} + r_{ij,k_j+1}^{b_ib_j}\right)\left(\vec{r}_{ij,k_j}^{b_ib_j} \times \vec{r}_{ij,k_j+1}^{b_ib_j}\right)}{r_{ij,k_j}^{b_ib_j} r_{ij,k_j+1}^{b_ib_j}\left(r_{ij,k_j}^{b_ib_j} r_{ij,k_j+1}^{b_ib_j} + \vec{r}_{ij,k_j}^{b_ib_j} \cdot \vec{r}_{ij,k_j+1}^{b_ib_j}\right)} \tag{3}$$

If the propeller rotates at speed $\vec{\omega}$ and has N_B blades, the total velocity at i is the superposition of the $N \times N_B$ HSV contributions, the free-stream $\vec{V}_\infty$, and the tangential velocity $\vec{V}_{t_i^{b_i}}$:

$$\vec{V}_{P_i^{b_i}} = \vec{V}_\infty + \vec{V}_{t_i^{b_i}} + \sum_{b_j=1}^{N_B}\sum_{j=1}^{N} \vec{V}_{HS_{ij}^{b_ib_j}} \tag{4}$$

$$\vec{V}_{t_i^{b_i}} = \vec{\omega} \times \vec{R}_i^{b_i} \tag{5}$$

i is initially placed over the hydrofoil $\frac{3}{4}c$, and a zero-normal-component is imposed at the overall velocity on this location (condition known as *Pistolesi Boundary Condition* - PBC [11]):

$$\vec{u}_{n_i^{b_i}} \cdot \vec{V}_{P_i^{b_i}} = 0 \rightarrow$$
$$\sum_{b_j=1}^{N_B} \sum_{j=1}^{N} \vec{u}_{n_i^{b_i}} \cdot \vec{V}_{HS_{ij}^{b_i b_j}} = -\vec{u}_{n_i^{b_i}} \cdot \left(\vec{V}_\infty + \vec{V}_{t_i^{b_i}} \right) \tag{6}$$

$\vec{u}_{n_i^{b_i}}$ is the normal-to-the-planform unit vector at i. Equation (6) can be more conveniently written using Eqn. (2):

$$\sum_{b_j=1}^{N_B} \sum_{j=1}^{N} m_{ij}^{b_i b_j} \Gamma_j^{b_j} = -4\pi \times W_{\infty_i^{b_i}} \tag{7}$$
$$m_{ij}^{b_i b_j} = \vec{u}_{n_i^{b_i}} \cdot \vec{v}_{ij}^{b_i b_j}$$
$$W_{\infty_i^{b_i}} = \vec{u}_{n_i^{b_i}} \cdot \left(\vec{V}_\infty + \vec{V}_{t_i^{b_i}} \right)$$

Since Eqn. (7) must be satisfied at the N control points of each of the N_B blades, a system of $N \times N_B$ equations is obtained for the propeller. Such system can be assembled in a matrix form:

$$\mathbf{M_P} \vec{\Gamma}_P = -\vec{W}_{\infty P} \tag{8}$$

$m_{ij}^{b_i b_j}$ are the elements of $\mathbf{M_P}$; note that $\mathbf{M_P}$ consists of influence sub-matrices $\mathbf{M^{b_i,b_j}}$, which account for the influence of blade b_j on blade b_i:

$$\mathbf{M_P} = \begin{bmatrix} \mathbf{M^{1,1}} & \cdots & \mathbf{M^{1,N_B}} \\ \vdots & \mathbf{M^{b_i,b_j}} & \vdots \\ \mathbf{M^{N_B,1}} & \cdots & \mathbf{M^{N_B,N_B}} \end{bmatrix} \tag{9}$$

Similarly, the circulation and free-stream arrays are assembled from these quantities of each of the blades:

$$\vec{\Gamma}_P = \begin{bmatrix} \Gamma_1^1 \\ \vdots \\ \Gamma_N^1 \\ \Gamma_1^2 \\ \vdots \\ \Gamma_N^{N_B} \end{bmatrix} \quad , \quad \vec{W}_{\infty P} = \begin{bmatrix} W_{\infty_1^1} \\ \vdots \\ W_{\infty_N^1} \\ W_{\infty_1^2} \\ \vdots \\ W_{\infty_N^{N_B}} \end{bmatrix} \tag{10}$$

Thus, the circulation distribution for all blades can be obtained at once by solving Eqn. (8). The Hydrodynamic forces (and corresponding coefficients) are calculated considering the influence of only the trailing vortices [7]:

$$\vec{V}_{TV_i^{b_i}} = \vec{V}_\infty + \vec{V}_{t_i^{b_i}} + \sum_{b_j=1}^{N_B} \sum_{j=1}^{N} \left(\vec{V}_{HS_{ij}^{b_i b_j}} - \vec{V}_{VS_{ij,\frac{N_s}{2}\,\frac{N_s}{2}+1}^{b_i b_j}} \right) \quad . \tag{11}$$

In addtion to Prandtl's hypothesis (the section lift at each wing section is equivalent to that of a similar section of an infinite wing having the same characteristics) [8], the hydrodynamic potential force at each control point is calculated with the application of the three dimensional version of Kutta-Joukowski theorem:

$$\Delta \vec{F}_i^{b_i} = \rho \Gamma_i^{b_i} \vec{V}_{TV_i^{b_i}} \times \vec{\delta}_{l_i^{b_i}} \rightarrow$$
$$|\Delta \vec{F}_i^{b_i}| = \rho |\Gamma_i^{b_i}| |\vec{V}_{TV_i^{b_i}}| |\vec{\delta}_{l_i^{b_i}}| \sin\theta_i^{b_i} \tag{12}$$

An equivalence between the definition of the 2-D normal force coefficient C_n and the Eqn. (12), an expression in term of $\Gamma_i^{b_i}$ is obtained:

$$C_{n_{Pot_i^{b_i}}} = \frac{\rho \Gamma_i^{b_i} |\vec{\delta}_{l_i^{b_i}}| \sin\theta_i^{b_i}}{\frac{1}{2}\rho |\vec{V}_{TV_i^{b_i}}| \delta A_i^{b_i}}. \tag{13}$$

which can be interpreted as a 'potential normal section force coefficient'.

Propeller Wake Model

Before presenting the changes for the nonlinear scheme, it is important to address the wake model.

Epps [12] showed that, for the case of a propeller with infinite blade number, Lerbs' wake model [2] was not consistent with the analytical expressions for the induced velocities. The author then proposed an improved wake model that agrees with the theoretical results and also improves the numerical consistency and robustness of the lifting-line algorithms; while in the classical wake model only one trailing vortex springs from each bound interior vortex point, in Epps' improved model two trailing vortices are shed from each bound segment. The HSV adopted by Epps is similar to the one of the present model and corroborates such choice. Therefore, the wake pitch angle $\beta_{w_{i,k*}^{b_i}}$ is obtained using Epps' assumption of a constant *hydrodynamic pitch* for each HSV:

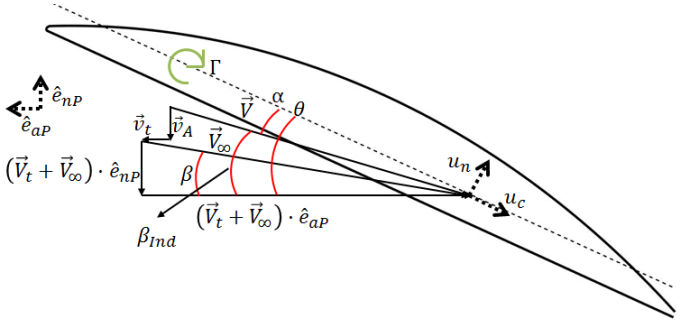

FIGURE 4. A propeller blade section and some of its important parameters.

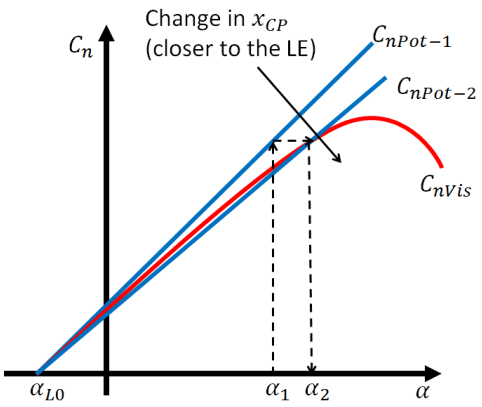

FIGURE 5. Scheme for the nonlinear formulation. Changing the control points locations changes the slope of the curve C_{n_α} accordingly.

$$|\vec{R}^{b_i}_{i,k_*}| \tan\left(\beta_{w^{b_i}_{i,k_*}}\left(\vec{R}^{b_i}_{i,k_*}\right)\right) = |\vec{R}^{b_i}_{i}| \tan\left(\beta^{b_i}_{Indi}\left(\vec{R}^{b_i}_{i}\right)\right) \tag{14}$$

for a control point i (of blade b_i) and corresponding bound vortex with index k_* ($* = i, i+1$). The pitch angle at the control point $\beta^{b_i}_i$ is calculated according to Eqn. (15) [6]:

$$\beta^{b_i}_{Indi}\left(\vec{R}^{b_i}_{i}\right) = \tan^{-1}\left[\frac{\left(\vec{V}_\infty + \sum_{b_j=1}^{N_B}\sum_{j=1}^{N}\vec{V}_{HS^{b_i b_j}_{ij}}\right)\cdot\vec{e}_{nP}}{\left(\vec{V}_\infty + \sum_{b_j=1}^{N_B}\sum_{j=1}^{N}\vec{V}_{HS^{b_i b_j}_{ij}}\right)\cdot\vec{e}_{aP} + |\vec{V}_{t^{b_i}_i}|}\right] \tag{15}$$

Equation (15) per se introduces nonlinearities in the problem as $\beta^{b_i}_{Indi}$ varies with the induced velocities (which, in turn, depend on $\vec{\Gamma}_P$). For the linear formulation $\vec{V}_{Ind^{b_i}_i} = \sum_{b_j=1}^{N_B}\sum_{j=1}^{N}\vec{V}_{HS^{b_i b_j}_{ij}}$ is assumed to be zero (i.e., $\beta^{b_i}_{Indi} = \beta^{b_i}_i$, as in Fig. 4). $\vec{e}_{aP}$ and $\vec{e}_{nP}$ are the unit vectors in the axial and normal directions of the global (propeller) reference frame.

Propeller Hub

The hub significantly influences the circulation distribution of the blade from the root until approximately half the span [6, 12]. Although more sophisticated methods can have satisfactorily accurate hub-models, the models available in the lifting-line formulations are rather simple. The model of Kerwin [6] was chosen in the present model; assuming that the hub has radius R_h, the radius of the image vortex $\vec{R}_{Im^{b_i}_{i,k_*}}$ is function of R_h and $\vec{R}^{b_i}_i$:

$$\vec{R}_{Im^{b_i}_{i,k_*}} = \frac{R_h^2}{|\vec{R}^{b_i}_{i,k_*}|}\frac{\vec{R}^{b_i}_{i,k_*}}{|\vec{R}^{b_i}_{i,k_*}|} \tag{16}$$

Note that the introduction of the hub model does not add unknowns to the problem since the image vortices have the same circulation of their 'real' counterparts. Finally the concentrated vortex that appears at the center of the hub is modelled as a Rankine vortex with a finite viscous core radius R_0 [13]; then, the resulting *pressure drag* can be easily computed:

$$D_P = \frac{\rho}{16\pi}\left(\log\frac{R_h}{R_0} + 3\right)(N_B\Gamma_h)^2 \tag{17}$$

Although R_0 must be estimated, variations from its precise value are not significant, as D_P depends on the natural logarithm of this quantity. Finally, the pressure drag must be accounted in the net propeller thrust.

Nonlinear Formulation

The present nonlinear scheme, used to incorporate real hydrofoil data on the PLL, is inspired on the work of Souza [9] (which is based on the work of Pepper & van Dam [14]) and it is an adaptation from the lifting-line theory for wings; viscosity is incorporated by moving the control points over the planform blade surface and imposing the PBC at the new locations. This process effectively changes the coefficients $m^{b_i b_j}_{ij}$ of $\mathbf{M_P}$ and, in practice, approximates the slope of the curve $C_n \times \alpha$ (C_{n_α}) to the slope of the curve $C_{nVis} \times \alpha$, $C_{n_{\alpha_{Vis}}}$ (Fig. 5).

The PBC was derived under the assumption of flat-plate airfoils [11], whose slopes C_{n_α} are 2π; if the blade sections are such

that $C_{n_\alpha} \neq 2\pi$, the chordwise control points (CP) locations $x_{cp_i^{b_i}}$ must be changed:

$$x_{cp_i^{b_i}} = \frac{3}{4}\frac{C_{n_\alpha i}}{2\pi}c_i \tag{18}$$

the normal and spanwise location must be changed accordingly so as to ensure the CPs remain over the blade planform. The linear process is repeated to obtain new estimates for $C_{n_{Pot_i}^{b_i}}$, a crucial step to ensure that PBC is satisfied. Next, the effective angles of attack are calculated considering the zero lift angles of attack α_{L0_i}:

$$\alpha_{eff_i^{b_i}} = \frac{C_{n_{Pot_i}^{b_i}}}{C_{n_\alpha i}} - \alpha_{L0_i} \tag{19}$$

The viscous effects are introduced by real hydrofoil data, as function of $\alpha_{eff_i^{b_i}}$ and section Reynolds number, $Re_i^{b_i}$. These data are generally obtained from experiments or numerical simulations:

$$C_{n_{Vis_i}^{b_i}} = C_{n_{Vis}}\left(\alpha_{eff_i^{b_i}}, Re_i^{b_i}\right). \tag{20}$$

$C_{n_{Vis_i}^{b_i}}$ are then compared with $C_{n_{Pot_i}^{b_i}}$ to check whether the differences are within a desirable tolerance. If a given convergence criterion is not satisfied, viscous forms of $C_{n_\alpha i}$, $C_{n_{\alpha_{Vis}} i}$ are calculated from $C_{n_{Vis_i}^{b_i}}$:

$$C_{n_{\alpha_{Vis}} i} = \frac{C_{n_{Vis_i}^{b_i}}}{\alpha_{eff_i^{b_i}} - \alpha_{L0_i}} \tag{21}$$

Equation (21) assumes that $C_{n_{\alpha_{Vis}} i}$ is linear; hence, the formulation is only suitable before stall region. Finally, $C_{n_\alpha i}$ are updated according to Eqn. (22):

$$C_{n_\alpha i} = \Omega C_{n_\alpha i} + (1-\Omega) C_{n_{\alpha_{Vis}} i} \tag{22}$$

in which Ω is an under relaxation factor that typically assumes the value of 0.8. The nonlinear process repeats until convergence is achieved. Note that the sectional viscous axial force coefficient C_c is obtained through the same 2-D data; this coefficient, however, is not used on the iterative process, but only on the post-processing calculations, and it is related to the hydrofoil viscous drag contribution on the overall thrust and torque: for inviscid cases, $C_c = 0$

Post Processing Calculations

The propeller thrust and torque coefficients (K_T and K_Q) are obtained from the values of C_n and C_c of each section. For each of these values, a corresponding transformation, in terms of the angle $\beta_{Indi}^{b_i}$ must be performed.

$$\begin{aligned} K_T &= \frac{\sum_{b_i=1}^{N_B}\sum_{i=1}^{N} |\vec{V}_{TV_i^{b_i}}|^2 \delta A_i \left[C_{n_i^{b_i}} \cos\left(\beta_{Indi}^{b_i}\right) - C_{c_i} \sin\left(\beta_{Indi}^{b_i}\right)\right]}{2\rho n^2 D^4} \\ K_Q &= \frac{\sum_{i=1}^{N} \vec{V}_{TV_i^{b_i}}|^2 |\vec{R}_i^{b_i}| \delta A_i \left[C_{n_i} \sin\left(\beta_{Indi}^{b_i}\right) + C_{c_i} \cos\left(\beta_{Indi}^{b_i}\right)\right]}{2n^2 D^5} \end{aligned} \tag{23}$$

with D the propeller diameter and n its rotation speed (RPM). As expected, the viscous drag increases the overall torque whilst it decreases the thrust.

Flowchart of the formulation

The flowchart of Fig. 6 illustrates the method described. The red lines are the path for the linear formulation, while the bold black ones the path for the nonlinear formulation:

RESULTS

For the ASME V&V 20 Committee [15], code and solution verifications must be performed to any numerical method in order to ensure its reliability. In this paper, verifications are done by systematically refining the discretization and either observing the behavior of the numerical solution, or comparing it with theoretical results, when available. For propellers, unfortunately, there are not many benchmarks available, what makes comparison with theoretical data more difficult; therefore, the majority of the following studies will verify the dependency of the solution on the mesh.

Solution Convergence Analysis

The error estimation is done through classical Richardson Extrapolation method. To perform the convergence analysis for the blades, systematic grid refinement is necessary; the coarsest blade discretization has 80 elements, whereas the finest has 452. The number of HSVs is consecutively increased by a ratio of approximately $\sqrt{2}$, value recommended by the committee [15]. The number of elements is represented by a refinement ratio r

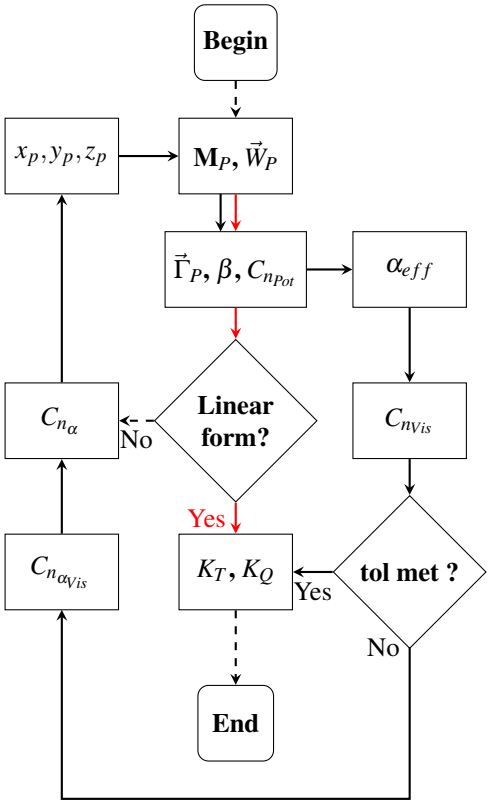

FIGURE 6. Flowchart of the PLL indicating the interaction between the linear and nonlinear formulations.

(according to Eqn. 24): $r = 1$ for the finest grid and $r = 0$ for an extrapolation in which the number of HSVs, N, tends to infinity.

$$r = \frac{h_N}{h_{N_{Max}}} \tag{24}$$

the variable h_N is a 'representative grid size' and, for the present formulation, it assumes the definition of Eqn. (25):

$$h_N = \frac{\sum_{i=1}^{N} |\vec{\delta}_{l_i}|}{N} \quad . \tag{25}$$

The behavior of the solution that is in the convergence region takes the form of Eqn. (26), in which f_{ext} is the extrapolated value, p the order of convergence, and C a constant. From this expression, a fitting curve is plotted against r.

$$f(h_N) = f_{ext} + C h_N^p \tag{26}$$

Therefore, the relative error is evaluated simply by calculating the difference

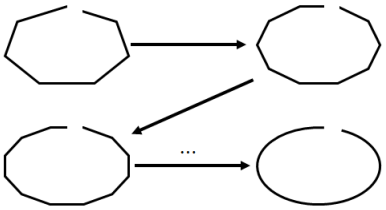

FIGURE 7. Schematics for the LVD convergence analysis.

$$E_{h_r} = |f_{ext} - f(h_N)|/|f_{ext}| \quad E_{h_a} = |f_{ext} - f(h_N)| \tag{27}$$

while the uncertainty u_{num} is estimated through a Grid Convergence Index (Eqns. 28 and 29):

$$GCI = \frac{F_S \times |f(h_{N_{max}}) - f\left(h_{(N_{max}-1)}\right)|}{\left[\frac{h_{N_{max}}}{h_{(N_{max}-1)}}\right]^p - 1} \tag{28}$$

$$u_{num_r} = GCI/(k \times f_{ext}) \quad u_{num_a} = GCI/k \tag{29}$$

The assigned values for F_s and k are 1.25 and 1.1, respectively, so that a conservative value for u_{num} can be estimated. In the current model, the wake can be refined by two ways: either increasing the number of straight segments per loop (called *Loop-Vortex Density* - LVD) or increasing the number of loops; prior to the HSVs mesh convergence analysis, a wake model convergence study is presented.

Wake Model: Loop-Vortex Density Although no analytic result exists for the velocity induced by a single helical loop, the convergence behavior of the induced velocity is verified as the loop-vortex density is increased (Fig. 7). The helix pitch angle β is approximately 17° and its radius $r_{hel} = 0.150\,m$. The probe is situated at $(0,0,0)$; the poorest simulation ($r \approx 22.5$) has 72 straight segments and the finest ($r = 1$) has 1630. Finally, δ_{l_i} is considered the length of each segment. Figure 8 shows the trend as a percentage of the extrapolated value.

p is found to be approximately 2, indicating second-order asymptotic convergence; moreover, numerical uncertainty is below 0.01%, so it is expected an insignificant influence from this uncertainty in the entire model uncertainty. For $N = 102$ ($r \approx 16.0$), the difference from the extrapolated value is under 0.01%. Therefore, it is expected that the velocity of a single helical loop can be accurately represented by $N \geq 102$.

Wake Model: Asymptotic behavior With a sufficiently accurate value for the LVD, the number of helical loops

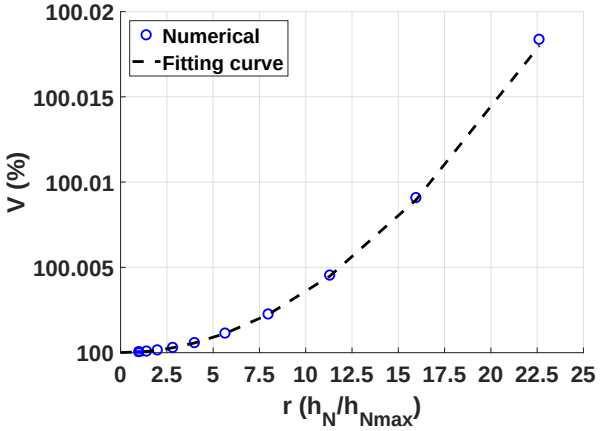

FIGURE 8. Convergence behavior of the LVD as the number of straight segments increases.

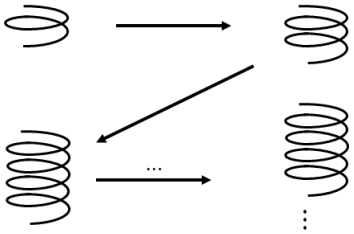

FIGURE 9. Schematics for the LVD convergence analysis.

N_H is gradually increased from 1 to 10 in order to evaluate the behavior of the induced velocity (Fig. 9); for this particular case, a different definition of h_N is used, since it is meaningless to define a mesh characteristic length:

$$h_{N_H} = \frac{1}{N_H} \tag{30}$$

Again, p is approximately 2, indicating a second-order asymptotic behavior for the increase in the number of loops as well. For the maximum number of loops, asymptotic behavior is already observed: increasing N_H further does not have any substantial influence. Moreover, for $r = 2$ ($N_H = 5$), the difference from the extrapolated value is within 0.05%, which is already satisfactory.

Wake Model: Wrench Formulas Wrench [17] presented analytical expressions for the velocities induced by helical HSVs having radii R along a radial distance R_c. The *Wrench formulas* are functions of N_B and the β. The present wake model is compared to such expressions.

Figure 11 is obtained fixing N_B to 5 and varying the pitch

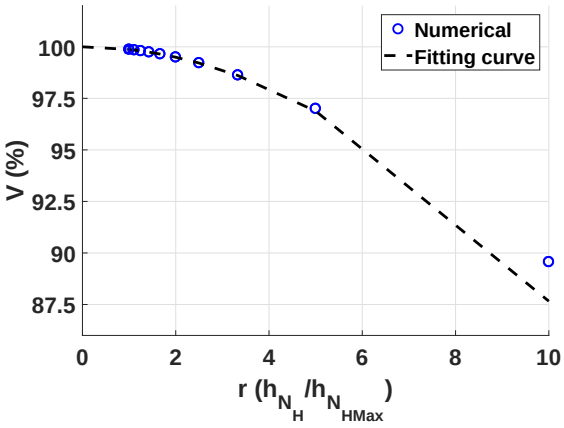

FIGURE 10. Convergence behavior of the increase in the number of loops to represent the propeller wake.

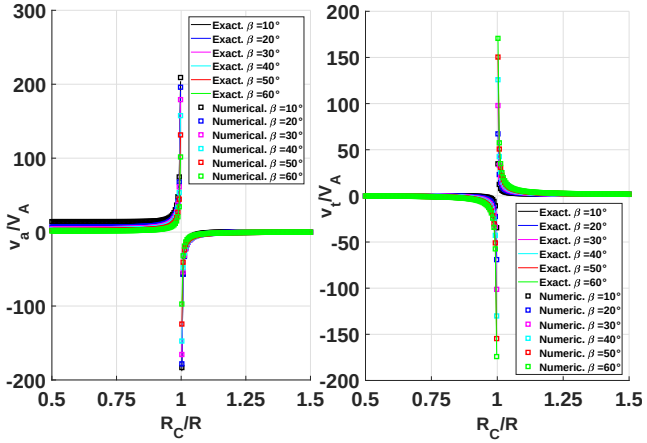

FIGURE 11. Comparison between numerical results and the Wrench formulas for $N_B = 5$ and several β.

angle from 10° to 60°. On the other hand, Fig. 12 is obtained fixing $\beta = 30°$ and varying N_B from 2 to 7. With $N_H = 5$ and $LVD = 102$, the numerical wake accurately reproduces the Wrench formulas.

Propeller Lifting-line Sequentially, the convergence of the blade discretization is studied. 3-Bladed Kaplan, KCA 312, and B-Troost propellers are used for the analysis. The type of discretization is also investigated, since there is evidence about the influence of clustering on convergence rate [8]; two clustering schemes were evaluated: Equal distribution for both HSVs and CPs (EHEP) [7] and sinusoidal distribution for both HSVs and CPs (CHCP) [8]. Figure 2 illustrates both the blades projected outlines and the clusterings. All combinations were stud-

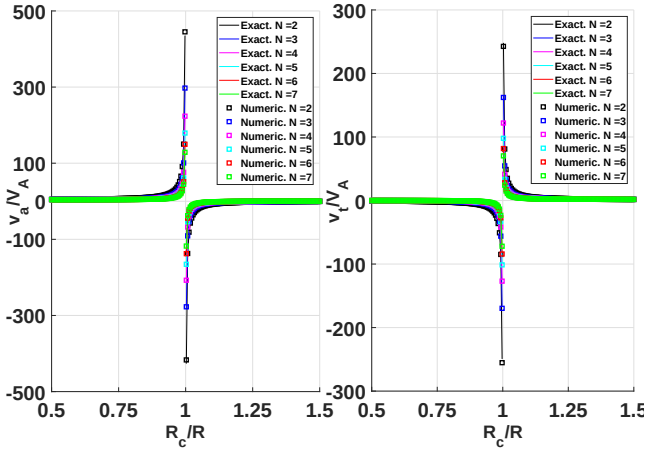

FIGURE 12. Comparison between numerical results and the Wrench formulas for $\beta = 30^\circ$ and several N_B.

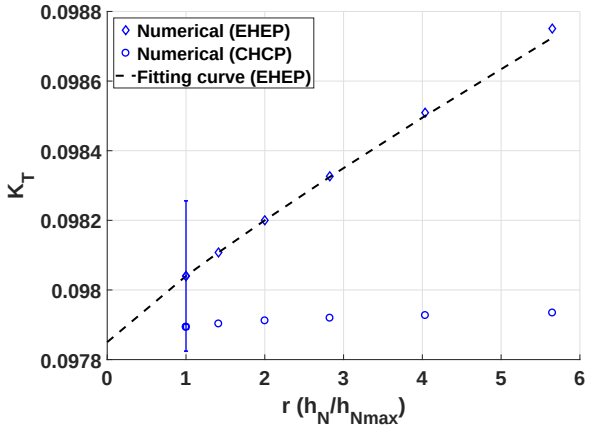

FIGURE 13. K_T versus r convergence analysis for the linear formulation.

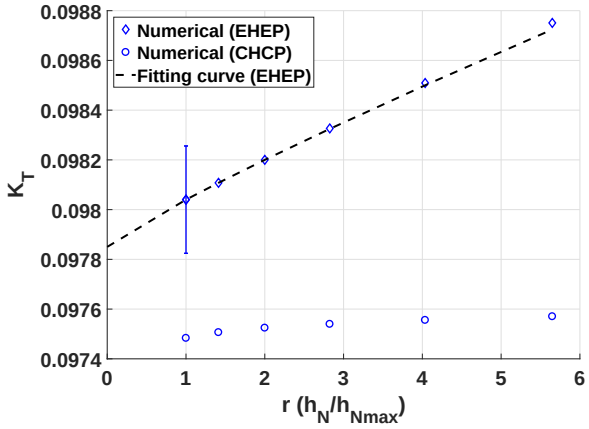

FIGURE 14. K_T versus r convergence analysis for the nonlinear formulation. numerical NACA0012 airfoil data was used [18].

ied and the convergence of K_T was analyzed for both linear and nonlinear formulations.

For the linear formulation, only the convergence of the KCA 312 propeller is presented (Fig. 13) since the results of the other two were either similar or better; the EHEP had no satisfactory convergence rate ($p \approx 0.88$), and the CHCP presented negligible variations of K_T: although no fitting curve was obtained, the reason was not a convergence issue, but rather Richardson Extrapolation was not a suitable verification procedure for the case.

In the nonlinear formulation, C_n and C_c data from the NACA0012 airfoil (obtained from XFOIL [18]) were used and the numerical tolerance (in terms of absolute and relative differences for C_n) was set to 1×10^{-4}. The convergence of the B-Troost propeller is presented (Fig. 14); Similarly, the EHEP presented the a convergence rate of $p \approx 0.88$, and the CHCP again had negligible variations of K_T; therefore, both the nonlinear formulation and the real airfoil data incorporated seem not to affect the order of convergence of the model.

CONCLUSION

This paper presents a novel propeller lifting-line model capable of simulating raked and/or skewed bladed propellers and of incorporating the influence of viscosity (from real hydrofoil coefficients) on thrust and torque. The latter is done through a nonlinear formulation that also accounts for the variations of the wake pitch angles according to the induced velocities. The model ensures that the Pistolesi Boundary Condition is satisfied over the control points. In terms of verification of the method, convergence analyses for the wake show that the model has an order of convergence close to 2. Moreover, the results from the Wrench Formulas are accurately reproduced. For the convergence analysis of the blade discretization, in the case of the linear formulation, the EHEP clustering presented an order of convergence of approximately 0.88, while the CHCP discretization did not return any convergence rate. The results for the CHCP, however, seem significantly better; this indicates that Richardson Extrapolation was probably not suitable to the analysis of this clustering scheme. For the nonlinear formulation, a similar trend was observed, indicating the suitability on the incorporation of the adaptive wake and the viscous effects.

The results obtained are substantial as they corroborate the broadening of the application range to PLL methods. As a future work, the authors intend to validate the model against experimental data for propellers, both under open water and nonsymmetric wake conditions (as it is the case of effective wakes left by hulls); the final purpose is to couple the PLL method with a commercial

CFD software in order to simulate hull-propeller assemblies in a robust, yet faster than in full CFD methods, manner.

ACKNOWLEDGMENT

The authors would like to acknowledge the financial support and scholarship granted by the Coordination for the Improvement of Higher Education Personnel (In Portuguese, Coordenação de Aperfeiçoamento de Pessoal de Nível Superior - CAPES), under project 1655506, and the Foundation for the institute for Technological Research (In Portuguese, Fundação de Apoio ao Instituto de Pesquisas Tecnológicas - FIPT).

REFERENCES

[1] Kawada, S., 1936. "Induced velocity by helical vortices". *J. Aeronaut. Sci*.

[2] Lerbs, H. W., 1952. "Moderately loaded propellers with a finite number of blades and arbitrary distribution of circulation.". *Trans SNAME*.

[3] Carlton, J., 2012. *Marine propellers and propulsion*. Butterworth-Heinemann.

[4] Epps, B., and Kimball, R., 2013. "Openprop v3: Open-source software for the design and analysis of marine propellers and horizontal-axis turbines". *N/A, Hanover, NH*.

[5] Stresses, I., and Summation, M. H. C. Propeller design with induction factors. publisher: Citeseer.

[6] Kerwin, J. E., and Hadler, J. B., 2010. "Principles of naval architecture series: Propulsion". *The Society of Naval Architects and Marine Engineers (SNAME)*.

[7] Katz, J., and Plotkin, A., 2001. *Low-speed aerodynamics*, Vol. 13. Cambridge University Press.

[8] Phillips, W., and Snyder, D., 2000. "Modern adaptation of prandtl's classic lifting-line theory". *Journal of Aircraft,* ***37***(4), pp. 662–670.

[9] de Souza, S. L., 2005. "Elaborao de uma metodologia para predio do coeficiente de sustentao mximo de asas flapeadas". Master's thesis, Instituto de Tecnolgico de Aeronutica.

[10] Chreim, J. R., Dantas, J. L. D., Burr, K. P., and Pimenta, M. d. M., 2017. "Viscous effects assessment through nonlinear lifting-line theory". In 24th ABCM International Congress of Mechanical Engineering, ABCM - Associacao Brasileira de Engenharia e Ciencias Mecanicas.

[11] Pistolesi, E., 1937. "Considerations respecting the mutual influence of systems of airfoils". In Collected Lectures of the 1937 Principal Meeting of the Lilienthal Society.

[12] Epps, B., 2017. "On the rotor lifting line wake model". *Journal of Ship Production and Design,* ***33***(1), pp. 31–45.

[13] Wang, M.-H., 1985. Hub effects in propeller design and analysis. Tech. rep., MASSACHUSETTS INST OF TECH CAMBRIDGE DEPT OF OCEAN ENGINEERING.

[14] Pepper, R. S., and van Dam, C., 1996. Design methodology for multi-element high-lift systems on subsonic civil transport aircraft. Tech. Rep. 19960054343, National Aeronautics and Space Administration, August.

[15] Committee, V. ., et al., 2009. "Standard for verification and validation in computational fluid dynamics and heat transfer". *American Society of Mechanical Engineers, New York*.

[16] Branlard, E., 2017. *Wind Turbine Aerodynamics and Vorticity-Based Methods: Fundamentals and Recent Applications*, Vol. 7. Springer.

[17] Wrench Jr, J., 1957. The calculation of propeller induction factors aml problem 69-54. Tech. rep., DAVID TAYLOR MODEL BASIN WASHINGTON DC.

[18] Drela, M., and Youngren, H., 2008. Xfoil, subsonic airfoil development system. URL http://web. mit. edu/drela/Public/web/xfoil.